

Diffusion of ellipsoids in laboratory two-dimensional turbulent flow ^{EP}

Cite as: Phys. Fluids **31**, 085116 (2019); <https://doi.org/10.1063/1.5113734>

Submitted: 06 June 2019 . Accepted: 31 July 2019 . Published Online: 26 August 2019

Jia Yang ^{ID}, Nicolas Francois ^{ID}, Horst Punzmann ^{ID}, Michael Shats ^{ID}, and Hua Xia ^{ID}

COLLECTIONS

^{EP} This paper was selected as an Editor's Pick



[View Online](#)




[Export Citation](#)



[CrossMark](#)

CAPTURE WHAT'S POSSIBLE
WITH OUR NEW PUBLISHING ACADEMY RESOURCES

Learn more 



Diffusion of ellipsoids in laboratory two-dimensional turbulent flow

Cite as: Phys. Fluids **31**, 085116 (2019); doi: [10.1063/1.5113734](https://doi.org/10.1063/1.5113734)

Submitted: 6 June 2019 • Accepted: 31 July 2019 •

Published Online: 26 August 2019



Jia Yang,  Nicolas Francois,  Horst Punzmann,  Michael Shats,  and Hua Xia^{a)} 

AFFILIATIONS

Research School of Physics and Engineering, The Australian National University, Canberra ACT 2601, Australia

^{a)}Electronic mail: hua.xia@anu.edu.au

ABSTRACT

We report on the transport properties and orientational dynamics of ellipsoidal objects advected by laboratory two-dimensional turbulence. It is found that ellipsoids of different sizes have preferential direction of transport, either along their major axes or minor axes. The two components of the ellipsoid diffusion coefficient depend on the ratio of the length of the ellipsoids along major axes aa to the turbulence forcing scale L_f . Large ellipsoids ($aa > L_f$) diffuse faster in the direction parallel to their major axes. In contrast, small ellipsoids diffuse faster in the direction transverse to their major axes. We study this transition vs the ratio aa/L_f and relate it to the coupling between translational and rotational motion of anisotropic objects. The features of the turbulent transport of ellipsoids can be understood by considering the interaction of these anisotropic objects with the underlying structure of two dimensional turbulent flows made of meandering coherent bundles.

Published under license by AIP Publishing. <https://doi.org/10.1063/1.5113734>

I. INTRODUCTION

Anisotropic particles are common in many industrial, natural, and environmental flows,¹ affecting processes such as paper making, pharmaceutical production, food processing, oceanic microbiome growth,² and even ocean light climate.³ In most practical cases, anisotropic particles are inertial particles, either because of the density mismatch between the particles and the fluid or because the particles have dimensions larger than a characteristic flow scale. Due to their geometric shape, anisotropic objects placed in a flow show a coupling between their translational and rotational degrees of freedom.⁴ Despite its importance, a complete description of the behavior of anisotropic objects in disordered flows is still lacking. Such a description is particularly challenging in turbulent flows. There has been extensive research based on DNS to study the rotational and translational motion of elongated fibers in isotropic turbulence.^{1,5,6} For thin rods with a high aspect ratio, the long axes of the rods align with the direction of the Lagrangian stretching in chaotic flows.^{7–9} The situation is further complicated with (1) finite aspect ratio of the ellipsoids¹⁰ and (2) the intricate tangle of highly convoluted material lines in turbulent flows.¹¹ A large part of the parameter range of anisotropic objects in turbulence remains unexplored⁴ and its exploration requires insights from experimental studies. Here, we are interested in the diffusion of ellipsoids with

intermediate aspect ratio and their interactions with the underlying turbulence.

This research topic also resonates with active research carried out on the transport of anisotropic particles in the so-called bacterial turbulence.¹² These chaotic flows are generated at microscopic scale by dense suspensions of bacteria.^{13–17} Interestingly, it has recently been reported that an ellipsoidal particle placed in bacterial turbulence shows an unusual coupling between its translational and orientational dynamics.¹⁸ Though bacterial turbulence exists at very low Reynolds number, it may share unexpected connections with hydrodynamics turbulence beyond the superficial visual resemblance. For instance, the emergence of collective effects in bacterial suspensions in confined geometries¹² is reminiscent of the phenomenology of self-organization observed in two-dimensional (2D) turbulence.^{19–21} Moreover, correlation in time and in space originating from the swarming motion of bacteria may be qualitatively similar to the behavior of coherent bundles of fluid particles recently reported in the structure of laboratory turbulent 2D flows.^{22,23}

In laboratory 2D turbulence, it has been shown that the single particle dispersion of fluid tracers is determined by the turbulence kinetic energy and by a single Lagrangian length scale (which is close to the turbulence forcing scale L_f).^{24–28} Studies of the dispersion of pairs of fluid tracers in such flows revealed that 2D turbulence

at moderate Reynolds numbers has an underlying Lagrangian fabric, which is composed of continuously evolving bundles of fluid particles.^{22,23} These bundles have a characteristic width that is proportional to the turbulence forcing scale L_f . Fluid particles moving together within such bundles execute collective random walks. Recently, it has been shown that these coherent bundles affect the transport properties of finite-size inertial objects,²⁹ where the scaling law of the turbulent diffusion coefficient of a disc depends on the size of the disc in comparison to the characteristic width of the bundles.

Here, we present results on transport properties of anisotropic objects, floating ellipsoids, in wave-driven 2D turbulence. We study the transport statistics and orientational dynamics of the ellipsoids advected by the turbulent flows. The translational dynamics of the ellipsoids strongly depend on the ratio of the size of the ellipsoid's major axis aa to the turbulence forcing scale L_f . Large ellipsoids ($aa > L_f$) diffuse faster in the direction parallel to their major axes. In contrast, small ellipsoids ($aa < L_f$) diffuse faster in the direction parallel to their minor axes. The latter effect resembles that reported in the case of an ellipsoid placed in bacterial turbulence.¹⁸ In this study, we show how the coupling between

the ellipsoids and the underlying structure of the flow is dependent on the ellipsoid's size aa . This allows us to discuss the differences observed between the turbulent transport of large and small ellipsoids.

II. EXPERIMENTAL SETUP

The experiments are conducted in turbulence generated at the water-air interface perturbed by Faraday waves.^{20,21,30} The wave frequencies vary from 30 Hz to 120 Hz corresponding to the flow forcing scales (L_f) in the range from 3 to 7.7 mm. The vertical acceleration a is characterized by the supercriticality parameter $\varepsilon = (a - a_{th})/a_{th}$ which in the reported experiments is in the range from 0.75 to 1.25 (here a_{th} is the threshold acceleration of parametric excitation of Faraday waves). The inertial objects under investigation are floating circular discs and ellipsoids. Floating objects were manufactured using a 3D Ultimaker 2 + printer with a thickness of 0.5 mm. The diameter of the discs and the major axes of the ellipsoids aa are varied from 3 mm to 40 mm. The minor axes bb of the ellipsoids depend on the aspect ratio (γ), which is defined as the ratio between minor axes of the ellipsoid and the major axes, $\gamma = bb/aa$. The aspect

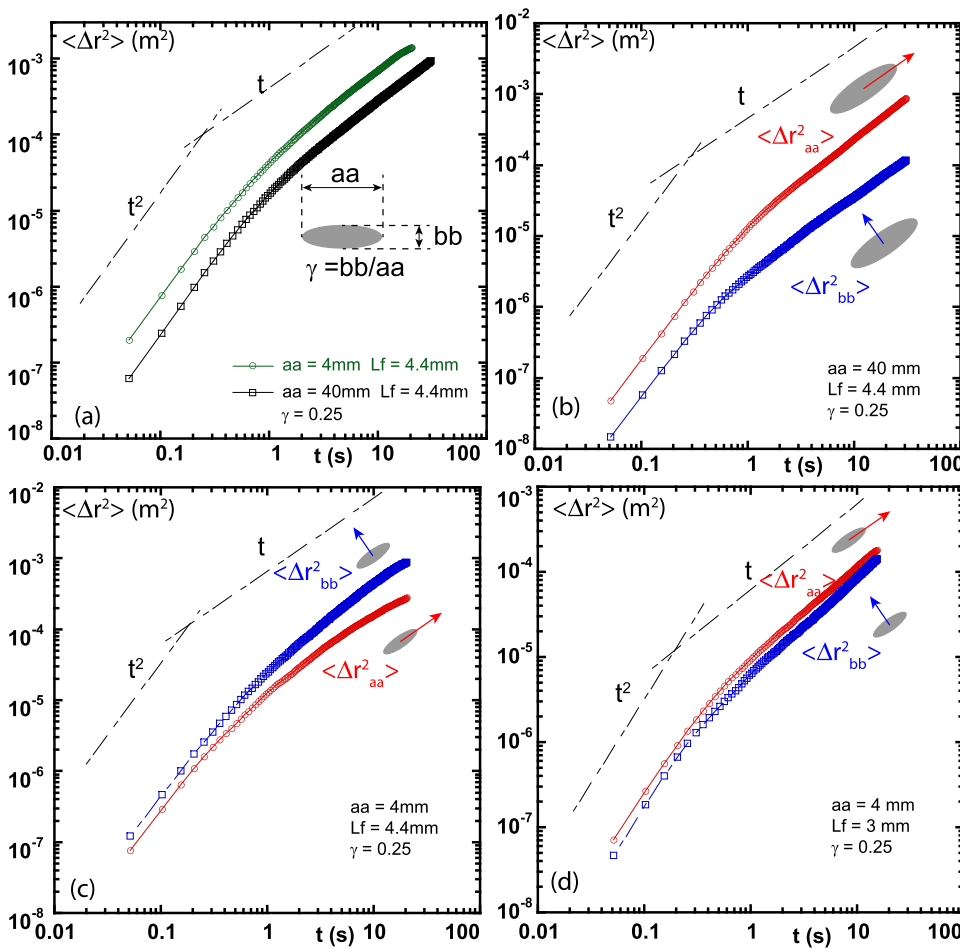


FIG. 1. (a) MSD of two ellipsoids in the laboratory frame of reference: $aa = 4$ mm (green) and $aa = 40$ mm (black), in a turbulent flow with $L_f = 4.4$ mm. MSD in the body frame of reference, $\langle \Delta r_{aa}^2 \rangle$ and $\langle \Delta r_{bb}^2 \rangle$ for: (b) $aa = 40$ mm, $L_f = 4.4$ mm, (c) $aa = 4$ mm, $L_f = 4.4$ mm, and (d) $aa = 4$ mm, $L_f = 3$ mm. The aspect ratio of the ellipsoids is $\gamma = 0.25$.

ratio varies from 0.1 to 1 (circular disc). For objects with aspect ratios equal to one (discs), a marker line was drawn on the top surface of the disc to track its rotation. All of the objects are washed carefully and immersed in water for 24 h to remove residual substances that can pollute the water. The top surface of the floating objects is coated with a thin layer of Teflon to prevent its wetting in the presence of steep waves.

The positions of the ellipsoids are recorded with an Andor Zyla camera at 20 fps for over 40 s. We measure the positions of the ellipsoids in the laboratory frame of reference (x and y) and their orientations with respect to the x axes, deriving the velocity vectors to study the transport dynamics of the objects.

III. DIFFUSION AND ORIENTATION OF THE ELLIPSOIDS

The statistically averaged mean squared displacement (MSD) of the ellipsoids in the laboratory frame of reference ($\langle \Delta r^2 \rangle$) is shown in Fig. 1(a). Here, $\Delta r = r(t) - r(t_0)$, where $r(t)$ is the position of the ellipsoid center along its trajectory, and $\langle \rangle$ denotes the ensemble averaging over many trajectories. For all the experiments, the ellipsoids show ballistic behavior at short times, $\langle \Delta r^2 \rangle \approx U^2 t^2$, and

diffusive behavior at long times, $\langle \Delta r^2 \rangle \approx 2Dt$. Here, D is the diffusion coefficient.

To investigate the effect of anisotropy, the MSD of the ellipsoids are also computed in the body frame of reference (along aa and bb). The diffusion along the major and minor axes are annotated as $\langle \Delta r_{aa}^2 \rangle$ and $\langle \Delta r_{bb}^2 \rangle$, respectively. Several examples of the body frame MSD for $aa = 40$ mm, 4 mm, and $L_f = 4.4$ and 3 mm are shown in Figs. 1(b)–1(d). In the body frame of reference, the MSDs are also diffusive at long time, satisfying

$$\langle \Delta r_{aa}^2 \rangle \approx D_{aa}t, \quad t \gg T_f, \quad (1)$$

$$\langle \Delta r_{bb}^2 \rangle \approx D_{bb}t, \quad t \gg T_f, \quad (2)$$

where aa and bb denotes quantities along major and minor axes, respectively.

There is a clear anisotropy in the body frame MSD of the ellipsoid, seen as the difference between $\langle \Delta r_{aa}^2 \rangle$ and $\langle \Delta r_{bb}^2 \rangle$. Moreover the results in Fig. 1 clearly show that the relative anisotropy (between the axis aa and bb) depends on the size of the ellipsoid. When the forcing scale L_f is fixed to $L_f = 4.4$ mm, ellipsoids with large major axes ($aa = 40$ mm) diffuse faster along their major axes, such

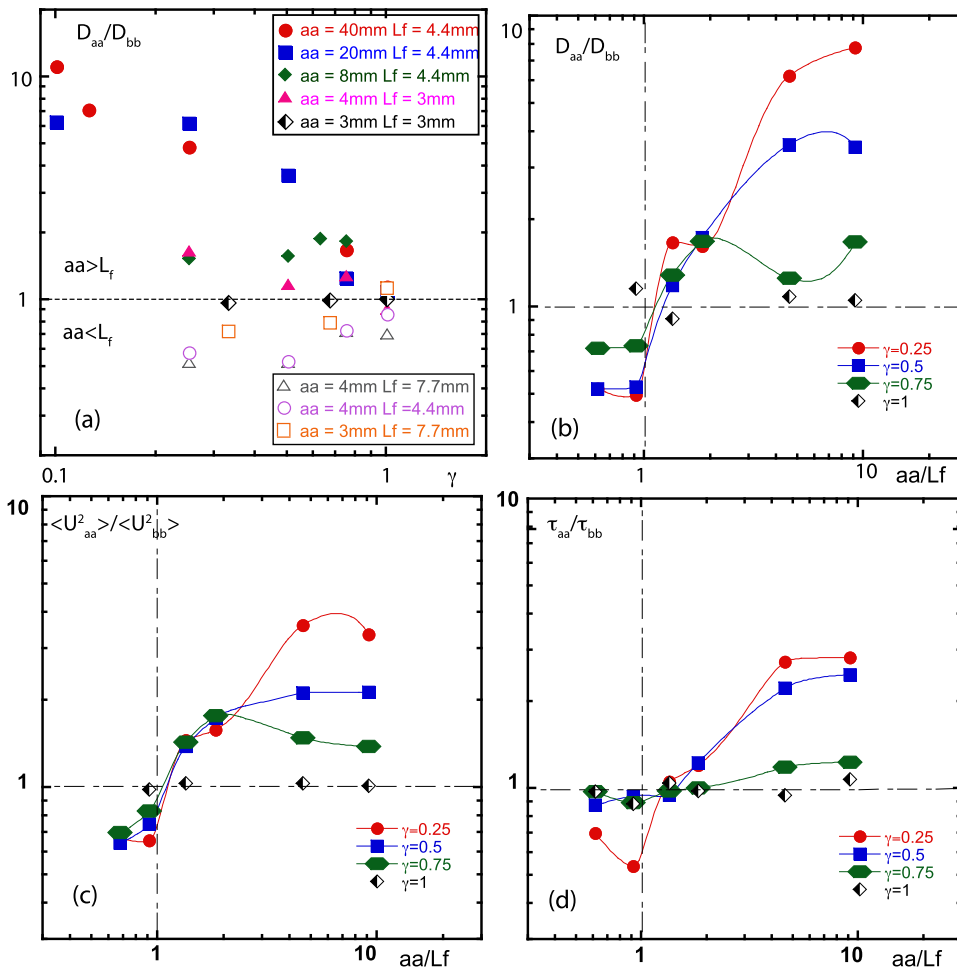


FIG. 2. (a) The ratio between the body-frame diffusion coefficient D_{aa}/D_{bb} obtained in different experimental conditions. (b) D_{aa}/D_{bb} , (c) $\langle U_{aa}^2 \rangle / \langle U_{bb}^2 \rangle$, and (d) τ_{aa}/τ_{bb} as a function of aa/L_f for various aspect ratios γ .

that $\langle \Delta r_{aa}^2 \rangle > \langle \Delta r_{bb}^2 \rangle$, Fig. 1(b). For smaller ellipsoids [$aa = 4$ mm, Fig. 1(c)], the situation is different: they diffuse faster along their short axes, such that $\langle \Delta r_{aa}^2 \rangle < \langle \Delta r_{bb}^2 \rangle$. A similar change in the preferential direction of the diffusion can also be achieved by keeping the same size of the ellipsoid $aa = 4$ mm, and by changing the forcing scale from 4.4 mm to 3 mm, as is seen from the comparison of Figs. 1(c) and 1(d).

Several questions arise from these observations. (1) Which scale or parameter determines the dispersion of ellipsoids? (2) Why larger ellipsoids diffuse faster along the major axes while the smaller ellipsoids diffuse faster in the direction of the minor axes?

To answer these questions, we compute the diffusion coefficients D_{aa} and D_{bb} from the body frame MSD. The ratios of the diffusion coefficients D_{aa}/D_{bb} are plotted for different experimental conditions in Fig. 2(a). When the aspect ratio of ellipsoids is nonzero, $\gamma \neq 1$, the ratio D_{aa}/D_{bb} takes values either below or above unity, as seen in Fig. 2(a). In all the experiments with the ellipsoid major axes larger than the forcing scale $aa > L_f$, this ratio is larger than one, $D_{aa}/D_{bb} > 1$, which means that ellipsoids diffuse faster along the major axes. However, in the experiments with the ellipsoid major axes smaller than the forcing scale $aa < L_f$, the ellipsoids diffuse faster along the short axes, $D_{aa}/D_{bb} < 1$. This anisotropic behavior vanishes when the aspect ratio is close to unity $\gamma \sim 1$.

The results show that the ratio aa/L_f determines the anisotropy measured in the diffusion coefficient. We refer to an ellipsoid as large if $aa/L_f > 1$, and we call it small if $aa/L_f < 1$. Figure 2(b) shows the same ratio D_{aa}/D_{bb} as a function of the ratio between these two scales aa/L_f . Two distinct regions of turbulent diffusion related to different aa/L_f are clearly seen: for small objects $D_{aa}/D_{bb} < 1$, while for large objects $D_{aa}/D_{bb} > 1$.

The ratio of D_{aa}/D_{bb} can be written as

$$\frac{D_{aa}}{D_{bb}} = \frac{\langle U_{aa}^2 \rangle \tau_{aa}}{\langle U_{bb}^2 \rangle \tau_{bb}}. \quad (3)$$

Here, U_{aa} and U_{bb} are the rms velocities along major and minor axes, respectively, and τ_{aa} and τ_{bb} are the corresponding Lagrangian autocorrelation times. Both parameters, the mean kinetic energy U^2 and the correlation time τ , are affected by the ratio aa/L_f [see Figs. 2(c) and 2(d)]. For either small or large objects, the difference in the diffusion coefficient is due to the combined effect of both the change in the mean energy and in the autocorrelation time.

To characterize further, the observed anisotropy of the diffusion coefficient, we turn to the orientational dynamics of the ellipsoids. We measure the orientation of the ellipsoid and the direction of the instantaneous velocity of the ellipsoid in the lab frame. θ_{aa} is defined as the angle between the ellipsoid major axes aa and the x axes in the laboratory frame and θ_V is the angle between its velocity vector and the x axes. If an ellipsoid moves in the direction of the major axes, the relative orientation angle of the ellipsoid, or the *angle of attack*, $\Delta\theta = |\theta_{aa} - \theta_V| \approx 0^\circ$, while $\Delta\theta = |\theta_{aa} - \theta_V| \approx 90^\circ$ corresponds to the transverse motion of ellipsoid.

The probability density functions of the angle of attack $|\theta_{aa} - \theta_V|$ for different ratios aa/L_f are shown in Figs. 3(a) and 3(b). For the same forcing scale of $L_f = 4.4$ mm, the cases of large (40 mm) and small (4 mm) ellipsoids are shown. The PDF of the 40 mm ellipsoids shows a peak at $|\theta_{aa} - \theta_V| = 0^\circ$, indicating that for large ellipsoids

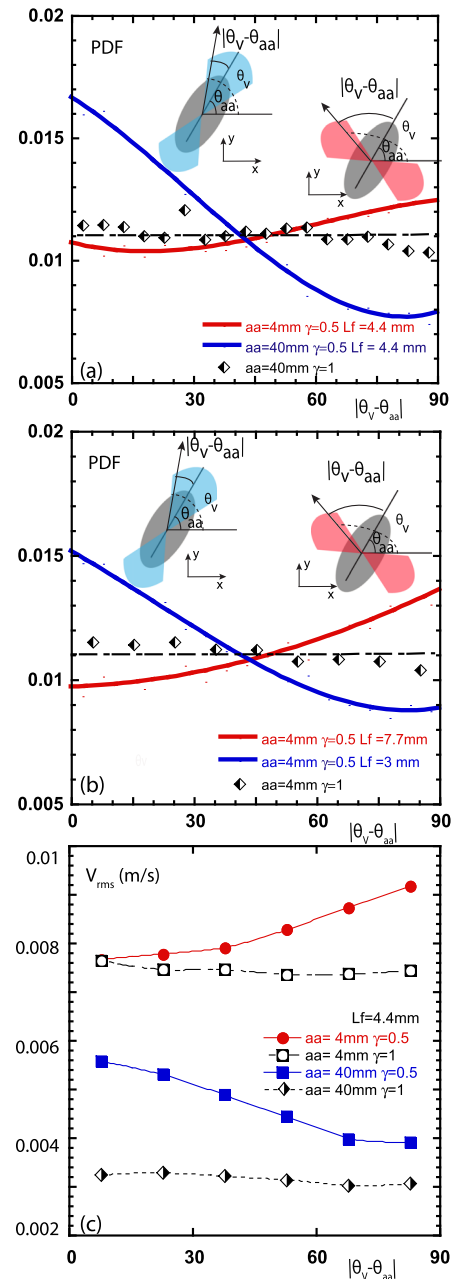


FIG. 3. PDF of the angle of attack $\Delta\theta = |\theta_V - \theta_{aa}|$ for (a) two different ellipsoid size aa , at the same flow forced at $L_f = 4.4$ mm, (b) the same ellipsoid size $aa = 4$ mm at two different forcing scale. The inserted illustrations show the ellipsoids' orientation and preferred direction of motion. (c) rms velocities of ellipsoids for different angles of attack $\Delta\theta = |\theta_V - \theta_{aa}|$. The experimental parameter is the same as that shown in (a). In all the plots, the corresponding experimental results of the circular discs (same aa , $\gamma = 1$) are also shown for comparison.

($aa/L_f > 1$), their movement is predominantly in the direction of the major axes, as illustrated in the inset. The PDF of the rms velocity of the ellipsoids for different angles of attack for the same experimental conditions is shown in Fig. 3(c) as the blue full square. It shows that

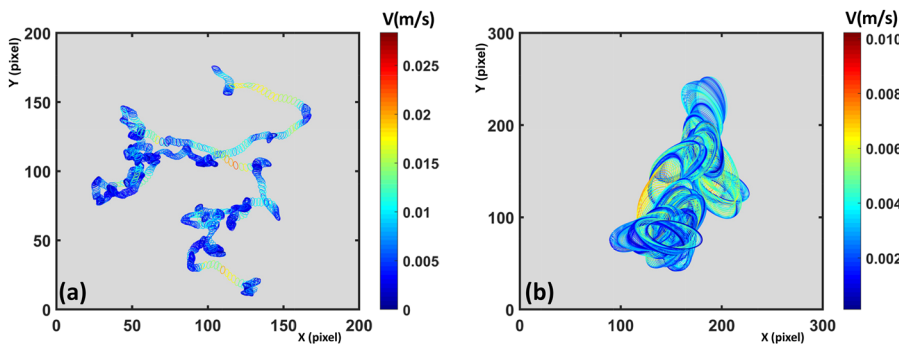


FIG. 4. (a) A typical trajectory of a 4 mm ellipsoid. The trajectory is recorded for a total time of 60 s with time interval between adjacent image 0.05 s. (b) A typical trajectory of a 40 mm ellipsoid. The trajectory is recorded for 60 s with time interval between adjacent images of 0.1 s. Both ellipsoids have the same aspect ratio $\gamma = 0.5$. Both trajectories are recorded in the flow forced at $\epsilon = 0.75$ and $L_f = 4.4$ mm.

ellipsoids moving in the direction of the major axes have higher rms velocities.

The preferred angles of attack of small ellipsoids are very different from those of large ellipsoids. For small ellipsoids with a major axes less than the forcing scale $aa/L_f < 1$ shown in Fig. 3(a) in red, $|\theta_{aa} - \theta_V|$ peaks at 90° . As illustrated in the inset of Fig. 3(a), in this case, the ellipsoids move transversely to the major axes. Similarly, the conditional rms velocity (averaged over different angular domains), shown in Fig. 3(c) (red full circles), is higher when the small ellipsoid's velocity is aligned with the minor axes, $|\theta_{aa} - \theta_V| \sim 90^\circ$.

Similar comparison of the PDFs of the angles of attack is obtained by keeping the same ellipsoid size and by changing the forcing scale of the flow. In Fig. 3(b), two PDFs of the angles of attack are

shown for a 4 mm ellipsoid in two different flow conditions. For the flow driven at $L_f = 3$ mm, the 4 mm ellipsoid behaves like a large one, with the preferred direction of movement along the major axes. When the flow is driven at $L_f = 7.7$ mm, the same ellipsoid behaves like a small one; its dominant direction is along the minor axes. In Figs. 3(a)–3(c), the reference cases of the circular discs ($\gamma = 1$) are also shown. The PDFs of angles of attack $|\theta_{aa} - \theta_V|$ for circular discs do not show any peaks, and they are flat within the range from 0° to 90° . The rms. velocity of the discs is also constant for any orientation of the disc.

The above statistical analysis suggests that (1) the ratio aa/L_f is a key parameter that determines the turbulent transport of ellipsoids, and (2) large ellipsoids diffuse faster and prefer to move along the major axes with higher velocities. In contrast,

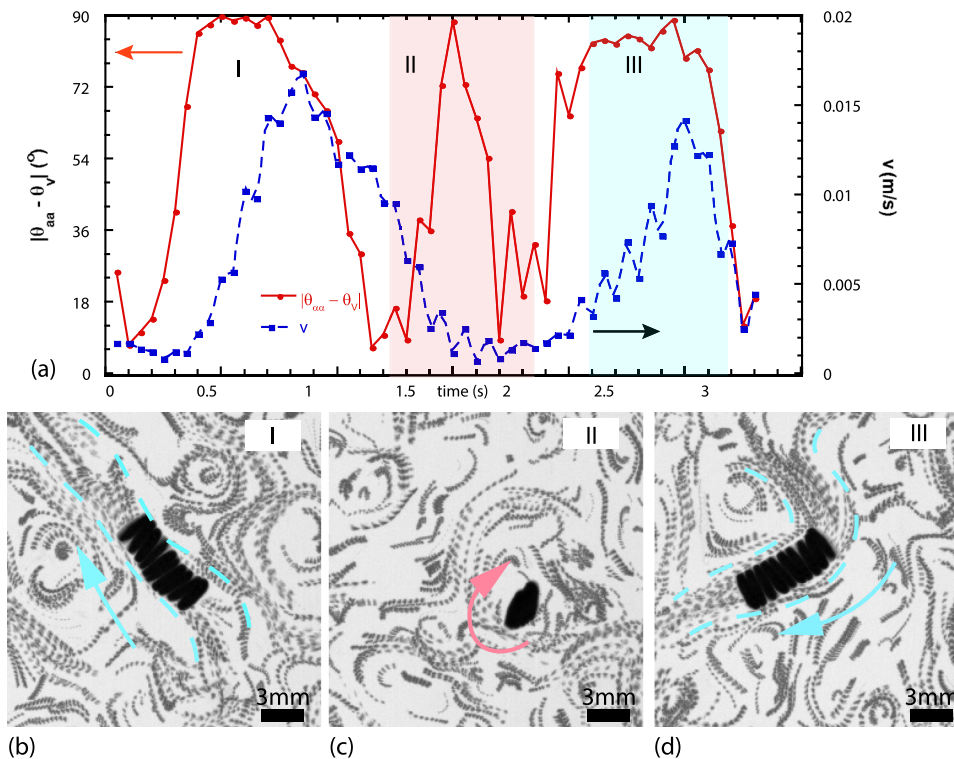


FIG. 5. (a) Temporal evolution of the translational velocity (blue dashed line) and the relative orientation of the object (δ_θ) (red solid line) for the 3 mm ellipsoid with $\gamma = 0.33$, the flow is forced at $L_f = 4.4$ mm. Three images (overlapping images of the ellipsoid and of the surrounding tracer particles) show the flight and trap events corresponding to the time intervals (b) I, (c) II, and (d) III. The dashed blue lines in (b) and (d) highlights the contour of the river-like structure that carries the small ellipsoid.

small ellipsoids move faster and prefer to diffuse along the minor axes.

IV. INTERACTION BETWEEN ELLIPSOIDS AND THE UNDERLYING FLOW

To gain further insights into the dynamics of ellipsoids, we visualized their trajectories and the turbulent fluid motion. Figures 4(a) and 4(b) show trajectories of ellipsoids of two different sizes tracked for 60 s, when the turbulent forcing scale is fixed at $L_f = 4.4$ mm. Both objects have the same aspect ratio of $\gamma = 0.5$. The time intervals between two consecutive positions of ellipsoids are 0.05 s for Fig. 4(a), and 0.1 s in Fig. 4(b). The symbol is calibrated to represent the actual size and the orientation of the ellipsoids. A color code indicates the velocity magnitude: higher velocity is orange-red, lower velocity is blue-black. Figure 4(b) shows the dynamics of a large ellipsoid with a major axis of $aa = 40$ mm. Both the translation and rotation of this large object show strong fluctuation and its overall behavior is reminiscent of the random walk of a Brownian ellipsoid. However, when $aa = 4$ mm and $L_f = 7.7$ mm, Fig. 4(a), which qualifies the ellipsoid as small, the trajectory shows a “flight-trap” behavior, similar to that reported for fluid particles.^{31,32} When a small ellipsoid is trapped, it rotates erratically and its position slowly fluctuates, as seen in Fig. 4(a). Such “traps” are followed by the long “flights” events seen as straight parts in the trajectory where the translation velocity is the highest [orange-red ellipsoids in Fig. 4(a)].

In Fig. 5, the small ellipsoid/flow coupling is studied by visualizing the structure of the flow surrounding the object. The temporal evolution of the translational velocity and of the relative orientation of the small ellipsoid is shown in Fig. 5(a). Two different regimes can be seen: a flight (time interval marked as I and III) and a trap (time interval II).

During the time interval I and III (the flight events), the ellipsoid’s translational velocity is aligned along its minor axis and its angle of attack remains high, $\Delta\theta \sim 90^\circ$. At the same time, the translational velocity gradually increases, as seen in the blue curve in Fig. 5(a) (blue shaded areas). Two images, Figs. 5(b) and 5(d), illustrate the flight event. Each panel shows time-elapsing images of the ellipsoid and of the tracer particles for 0.5 s. The tracer particles reveal coherent bundles in the turbulent flow, similar to those described in Refs. 22 and 23. These bundles interact with the ellipsoid, pushing it along its minor axis. The most effective momentum transfer occurs when the minor axis of the ellipsoid is aligned with the coherent bundle; this explains the correlations observed in Fig. 4(a) between high velocity events (orange-red) and the ellipsoid moving transversely. This observation is also consistent with the statistical result showing that the rms velocity of the small objects is higher when the velocity direction is aligned along the minor axes, Fig. 3(c).

As has been shown in Refs. 22 and 23, the coherent bundles have a finite life time due to their constant interaction with surrounding bundles. During a flight event [Figs. 5(b) and 5(d)], an ellipsoid is carried by the bundle only for a finite time until it is trapped again, as illustrated by the pink shaded area (II). When the ellipsoid becomes trapped, its translational velocity decreases and stays low while the angles of attack fluctuates strongly in the range $(0^\circ, 90^\circ)$ due to the erratic rotation of the ellipsoid around the trapping point, as can be seen in the image in Fig. 5(c). It

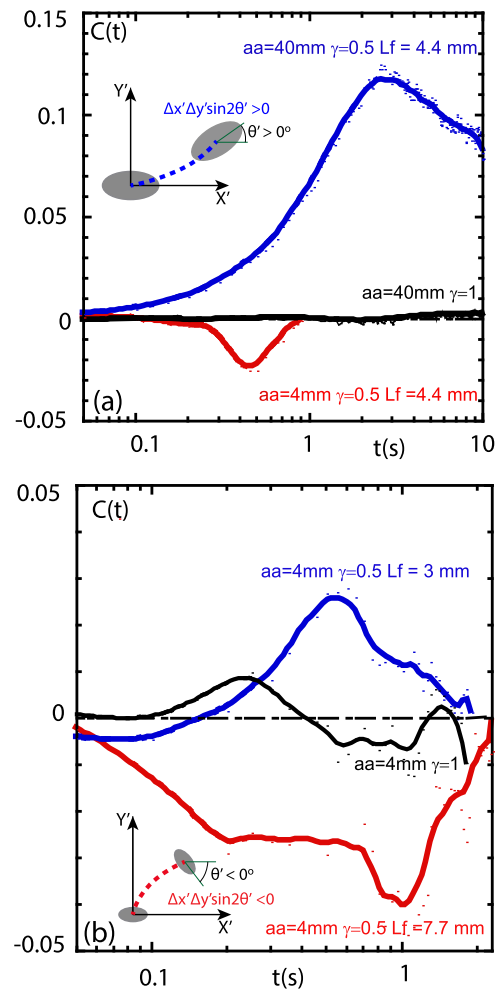


FIG. 6. The mixed cross correlation function $C(t)$ for different experimental conditions. (a) Different sizes of ellipsoids $aa = 40$ mm and $aa = 4$ mm, at forcing scale of $L_f = 4.4$ mm. (b) The same ellipsoids $aa = 4$ mm $\gamma = 0.5$ at different forcing scales of $L_f = 3$ mm and 7.7 mm. In both plots, the corresponding MCC for circular disc is shown.

shows that the ellipsoid is trapped locally and it is rotating. Since the flow consists of constantly interacting bundles, the ellipsoid in a trapping region escapes the trap due to an impacting coherent bundle. This detrapping event leads to another flight event [Fig. 5(d)]. The most effective detrapping events occur when a bundle impacts the ellipsoid transversely along its minor axis. This phenomenology of short trap-long flight events is consistent with the fact that small ellipsoids move principally along their minor axes.

The alignment of the ellipsoid axes with their velocity vectors is governed by a coupling between their translational and rotational motion. A dimensionless mixed cross correlation function¹⁸ was proposed to characterize such coupling,

$$C(t) = \langle \Delta x' \Delta y' \sin 2\theta' \rangle / \langle \Delta x'^2 + \Delta y'^2 \rangle. \quad (4)$$

The mixed cross correlation (MCC) function $C(t)$ gives a statistical ensemble average of the coupling between the translational motion in laboratory frame and the rotation of the objects (θ'), $\theta' \in [-90^\circ, 90^\circ]$. To compute the MCC, we redefine the coordinates in the laboratory frame according to the initial orientation of ellipsoids on each trajectory, such that all the ellipsoids will start from point (0, 0) position with the angle between the new x-axis and the ellipsoid's major axis, $\theta'_{i0} = 0^\circ$. The displacements in this new laboratory frame of reference are $\Delta x'$ and $\Delta y'$. When an ellipsoid diffuses along its major axis, it leads to a positive coupling $\langle \Delta x' \Delta y' \sin 2\theta' \rangle > 0$ [see the schematic trajectory in the insert of Fig. 6(a)]. On the other hand, a negative mixed cross correlation function $\langle \Delta x' \Delta y' \sin 2\theta' \rangle < 0$ indicates that the ellipsoid translates along the minor axis of the ellipsoid [insert of Fig. 6(b)], leading to a negative coupling.

The MCC's for two ellipsoids ($aa = 40$ mm and 4 mm, $\gamma = 0.5$) and a circular disc ($aa = 40$ mm, $\gamma = 1$) under the same flow conditions ($L_f = 4.4$ mm) are shown in Fig. 6(a). The MCC for a circular disc is close to zero, as would be expected for an object with independent translational and rotational degrees of freedom. $C(t)$ deviates from zero for both ellipsoids indicating a coupling between the two degrees of freedom. The translation and rotation of the ellipsoid with $aa/L_f > 1$ is positively coupled, $C > 0$. The MCC shows a change from positive to negative with the change in aa/L_f : a negative coupling ($C < 0$) arises when $aa/L_f < 1$. Similar to the change of the object size, a transition from positive to negative coupling can be achieved by changing the forcing scale of the flow. As shown in Fig. 6(b), for the same ellipsoids with $aa = 4$ mm and $\gamma = 0.5$, the MCC changes from positive to negative when the forcing scale of the flow changes from $L_f = 3$ mm to 7.7 mm. For the circular disc, the MCC fluctuates but stays close to zero. The negative "anomalous" coupling observed for the small ellipsoids confirms that a small ellipsoid advected by the turbulence moves principally along a direction parallel to its minor axis.

V. DISCUSSION

The results shown in this study allow us to draw interesting analogies between the turbulent transport of ellipsoids and the behavior of microscopic ellipsoids placed in a thermal bath or in bacterial turbulence.

The Brownian motion of an ellipsoid placed in contact with a thermal bath has been considered theoretically.^{33–35} Its motion is characterized by two friction coefficients, γ_{aa} along the long axes and γ_{bb} along the short axes. The friction coefficient is larger along the short axes, thus giving anisotropic diffusion with larger diffusion coefficient along the long axes. The preferential diffusion of such a Brownian ellipsoid along the long axes was confirmed in water confined to two dimensions.³⁶ In the strongly nonequilibrium turbulent flows studied here, the turbulent transport of large ellipsoids shows analogies with the Brownian motion of microscopic ellipsoids. Large ellipsoids ($aa > L_f$) diffuse faster in the direction parallel to their major axes. These large ellipsoids interact with many underlying coherent bundles. This interaction with many degrees of freedom might be the source of the Brownian-like behavior. However, there are some important differences compared with the behavior of Brownian objects in thermal equilibrium. For instance in our macroscopic system, it was shown that not only the dissipation

(characterized by the Lagrangian time scale τ) but also the energy of the ellipsoid is function of its orientation. Indeed, the rms velocity of the large ellipsoid is higher when its velocity direction is aligned with its major axis.

Small ellipsoids ($aa < L_f$) placed in wave-driven turbulence diffuse faster in the direction transverse to their major axes. This behavior resembles that reported in the case of an ellipsoid placed in bacterial turbulence.¹⁸ More precisely, an unusual coupling between translation and rotation of ellipsoidal objects has been reported in dense bacterial suspensions. It was shown that above a certain concentration, a negative coupling of the translational and orientational dynamics arise: the microscopic ellipsoid moves on average principally along its minor axis. As mentioned above, such transport is forbidden for the Brownian motion of ellipsoids in thermal equilibrium. For this reason, this coupling was termed anomalous. This anomalous coupling and diffusion was attributed to the mechanical properties of swimming microorganisms, being pushers or pullers, and to the corresponding strain generated by the active fluid.³⁷ We note that dense suspensions of bacteria have a tendency to produce swarming motion.^{13–17} This swarming motion of bacteria seems to share some similarities with the behavior of coherent bundles of fluid particles recently reported in laboratory turbulent 2D flows.^{22,23} This similarity creates a tantalizing bridge between these two very distinct systems and highlights how the transport properties of chaotic flows are deeply connected to their Lagrangian structures.

In our experiments, the flow-object coupling results in trajectories of small ellipsoids showing a "flight-trap" behavior, similar to the behavior of fluid particles.^{31,32} When a small ellipsoid is trapped, it rotates erratically and its position slowly fluctuates. The most efficient detrapping events occur when a bundle impacts with it transversely along its minor axis. Indeed, the most effective momentum transfer occurs when the minor axis of the ellipsoid is aligned with the impact direction of the coherent bundle. The traps are followed by long flights events during which the ellipsoid is carried by the fluid bundle. During the flight, the ellipsoid moves transversely and gains a substantial amount of kinetic energy. The flight event is followed by another trap event due to the finite life time of the bundle. This sequential phenomenology is consistent with the statistical description of the turbulent transport of small ellipsoid.

VI. CONCLUSIONS

We present experimental results on the transport of floating ellipsoids placed in wave-driven 2D turbulence. The turbulent transport of these anisotropic objects is strongly affected by the underlying fabric of the flow. This fabric is made of a network of coherent river-like structures with a characteristic width close to the turbulent flow forcing scale L_f . Large ellipsoids ($aa > L_f$) interact with many bundles and as a result diffuse faster in the direction parallel to their major axes, a behavior reminiscent of the dynamics of an ellipsoid undergoing a Brownian motion. In contrast, small ellipsoids diffuse faster in the direction transverse to their major axes. We show that this coupling between the translational and rotational diffusion arises as a result of the advection of the small ellipsoid by a single coherent bundle at a time.

ACKNOWLEDGMENTS

This work was supported by the Australian Research Council's Discovery Projects funding scheme Grant Nos. DP160100863 and DP190100406. H.X. acknowledges support from the Australian Research Council's Future Fellowship (Grant No. FT140100067). N.F. acknowledges support by the Australian Research Council's DECRA award (Grant No. DE160100742). J.Y. acknowledges valuable supports and discussions from Jean-Baptiste Gorce.

REFERENCES

- ¹G. A. Voth and A. Soldati, "Anisotropic particles in turbulence," *Annu. Rev. Fluid Mech.* **49**, 249–276 (2017).
- ²K. R. Conley and K. R. Sutherland, "Particle shape impacts export and fate in the ocean through interactions with the globally abundant appendicularian *oikopleura dioica*," *PLoS One* **12**, e0183105 (2017).
- ³J. R. Seymour, M. Luhr, W. M. Durham, J. G. Mitchell, A. Macke, R. Stocker *et al.*, "Microbial alignment in flow changes ocean light climate," *Proc. Natl. Acad. Sci. U. S. A.* **108**, 3860–3864 (2011).
- ⁴H. Berthet, M. Fermigier, and A. Lindner, "Single fiber transport in a confined channel: Microfluidic experiments and numerical study," *Phys. Fluids* **25**, 103601 (2013).
- ⁵M. Shin and D. L. Koch, "Rotational and translational dispersion of fibres in isotropic turbulent flows," *J. Fluid Mech.* **540**, 143–173 (2005).
- ⁶A. Pumir and M. Wilkinson, "Orientation statistics of small particles in turbulence," *New J. Phys.* **13**, 093030 (2011).
- ⁷S. Parsa, J. S. Guasto, M. Kishore, N. T. Ouellette, J. Gollub, and G. A. Voth, "Rotation and alignment of rods in two-dimensional chaotic flow," *Phys. Fluids* **23**, 043302 (2011).
- ⁸R. Ni, N. T. Ouellette, and G. A. Voth, "Alignment of vorticity and rods with Lagrangian fluid stretching in turbulence," *J. Fluid Mech.* **743**, R3 (2014).
- ⁹L. Zhao and H. I. Andersson, "Why spheroids orient preferentially in near-wall turbulence," *J. Fluid Mech.* **807**, 221–234 (2016).
- ¹⁰S. Parsa, E. Calzavarini, F. Toschi, and G. A. Voth, "Rotation rate of rods in turbulent fluid flow," *Phys. Rev. Lett.* **109**, 134501 (2012).
- ¹¹M. Mathur, G. Haller, T. Peacock, J. E. Ruppert-Felsot, and H. L. Swinney, "Uncovering the Lagrangian skeleton of turbulence," *Phys. Rev. Lett.* **98**, 144502 (2007).
- ¹²C. Bechinger, R. Di Leonardo, H. Löwen, C. Reichhardt, G. Volpe, and G. Volpe, "Active particles in complex and crowded environments," *Rev. Mod. Phys.* **88**, 045006 (2016).
- ¹³N. H. Mendelson, A. Bourque, K. Wilkening, K. R. Anderson, and J. C. Watkins, "Organized cell swimming motions in *Bacillus subtilis* colonies: Patterns of short-lived whirls and jets," *J. Bacteriol.* **181**, 600–609 (1999).
- ¹⁴C. Dombrowski, L. Cisneros, S. Chatkaew, R. E. Goldstein, and J. O. Kessler, "Self-concentration and large-scale coherence in bacterial dynamics," *Phys. Rev. Lett.* **93**, 098103 (2004).
- ¹⁵H. H. Wensink, J. Dunkel, S. Heidenreich, K. Drescher, R. E. Goldstein, H. Löwen, and J. M. Yeomans, "Meso-scale turbulence in living fluids," *Proc. Natl. Acad. Sci. U. S. A.* **109**, 14308–14313 (2012).
- ¹⁶A. Sokolov and I. S. Aranson, "Physical properties of collective motion in suspensions of bacteria," *Phys. Rev. Lett.* **109**, 248109 (2012).
- ¹⁷J. Dunkel, S. Heidenreich, K. Drescher, H. H. Wensink, M. Bär, and R. E. Goldstein, "Fluid dynamics of bacterial turbulence," *Phys. Rev. Lett.* **110**, 228102 (2013).
- ¹⁸Y. Peng, L. Lai, Y.-S. Tai, K. Zhang, X. Xu, and X. Cheng, "Diffusion of ellipsoids in bacterial suspensions," *Phys. Rev. Lett.* **116**, 068303 (2016).
- ¹⁹H. Xia, M. Shats, and G. Falkovich, "Spectrally condensed turbulence in thin layers," *Phys. Fluids* **21**, 125101 (2009).
- ²⁰H. Xia and N. Francois, "Two-dimensional turbulence in three-dimensional flows," *Phys. Fluids* **29**, 111107 (2017).
- ²¹N. Francois, H. Xia, H. Punzmann, and M. Shats, "Inverse energy cascade and emergence of large coherent vortices in turbulence driven by faraday waves," *Phys. Rev. Lett.* **110**, 194501 (2013).
- ²²H. Xia, N. Francois, B. Faber, H. Punzmann, and M. Shats, "Local anisotropy of laboratory two-dimensional turbulence affects pair dispersion," *Phys. Fluids* **31**, 025111 (2019).
- ²³N. Francois, H. Xia, H. Punzmann, and M. Shats, "Rectification of chaotic fluid motion in two-dimensional turbulence," *Phys. Rev. Fluids* **3**, 124602 (2018).
- ²⁴H. Xia, N. Francois, H. Punzmann, and M. Shats, "Lagrangian scale of particle dispersion in turbulence," *Nat. Commun.* **4**, 2013 (2013).
- ²⁵H. Xia, N. Francois, H. Punzmann, and M. Shats, "Taylor particle dispersion during transition to fully developed two-dimensional turbulence," *Phys. Rev. Lett.* **112**, 104501 (2014).
- ²⁶N. Francois, H. Xia, H. Punzmann, and M. Shats, "Wave-particle interaction in the faraday waves," *Eur. Phys. J. E* **38**, 106 (2015).
- ²⁷N. Francois, H. Xia, H. Punzmann, T. Combriat, and M. Shats, "Inhibition of wave-driven two-dimensional turbulence by viscoelastic films of proteins," *Phys. Rev. E* **92**, 023027 (2015).
- ²⁸N. Francois, H. Xia, H. Punzmann, B. Faber, and M. Shats, "Braid entropy of two-dimensional turbulence," *Sci. Rep.* **5**, 18564 (2015).
- ²⁹H. Xia, N. Francois, H. Punzmann, and M. Shats, "Tunable diffusion in wave-driven two-dimensional turbulence," *J. Fluid Mech.* **865**, 811–830 (2019).
- ³⁰A. Von Kameke, F. Huhn, G. Fernández-García, A. Munuzuri, and V. Pérez-Muñuzuri, "Double cascade turbulence and Richardson dispersion in a horizontal fluid flow induced by faraday waves," *Phys. Rev. Lett.* **107**, 074502 (2011).
- ³¹N. Francois, H. Xia, H. Punzmann, S. Ramsden, and M. Shats, "Three-dimensional fluid motion in faraday waves: Creation of vorticity and generation of two-dimensional turbulence," *Phys. Rev. X* **4**, 021021 (2014).
- ³²A. E. Hansen, E. Schröder, P. Alström, J. S. Andersen, and M. T. Levinsen, "Fractal particle trajectories in capillary waves: Imprint of wavelength," *Phys. Rev. Lett.* **79**, 1845 (1997).
- ³³F. Perrin, "Brownian motion of an ellipsoid-I. Dispersed dielectric for ellipsoidal molecules," *J. Phys. Radium* **5**, 497–511 (1934).
- ³⁴G. B. Jeffery, "The motion of ellipsoidal particles immersed in a viscous fluid," *Proc. R. Soc. A* **102**, 161–179 (1922).
- ³⁵J. Happel and H. Brenner, *Low Reynolds Number Hydrodynamics: With Special Applications to Particulate Media* (Springer Science & Business Media, 2012), Vol. 1.
- ³⁶Y. Han, A. Alsayed, M. Nobili, J. Zhang, T. C. Lubensky, and A. G. Yodh, "Brownian motion of an ellipsoid," *Science* **314**, 626–630 (2006).
- ³⁷O. Yang, Y. Peng, Z. Liu, C. Tang, X. Xu, and X. Cheng, "Dynamics of ellipsoidal tracers in swimming algal suspensions," *Phys. Rev. E* **94**, 042601 (2016).